RSC Advances

ROYAL SOCIETY OF CHEMISTRY

www.rsc.org/advances

RSCPublishing

ARTICLE

Au nanoflower@SiO_2@CdTe/CdS/ZnS quantum dots multi-functional nanoprobe for photothermal treatment and cellular imaging

Tongtong Jiang,[a] Naiqiang Yin,[a] Ling Liu,[a] Jiangluqi Song,[a] Qianpeng Huang,[b] Lixin Zhu,*[b] Xiaoliang Xu*[a]

Au nanoparticle@SiO_2@CdTe/CdS/ZnS quantum dots (QDs) composite structures were synthesized by liquid phase synthesis method. In this paper, three steps were adopted to gradually grow PVP-stabilized Au seed with which PVP-stabilized Au nanoflowers (NFs) structures was successfully synthesized. For the sack of controlling the distance of Au NF and QDs, silica was used as the shell material for coating Au NF. The applications of this multi-functional nanoprobe in photothermal treatment and bio-labeling were demonstrated on the MCF-7 and MDA-MB-231 breast cancer cells labeled with Au NF@SiO_2@QDs. The experimental results of viability staining indicate that Au NF@SiO_2@QDs composites with the excitation threshold of the photothermal effect only 1.0W/cm^2 exhibit excellent photothermal conversion efficiency owing to the large absorption cross sections of Au NF. Compared with pure QDs, the fluorescence efficiency of Au NF@SiO_2@QDs was increased by 40%, which could be attributed to localized surface plasmon enhanced dipole radiation. The fluorescence imaging results reveal that Au NF@SiO_2@QDs targeted to the membrane of cancer cell showing strong fluorescence. Therefore, it can be concluded that composite structure combines the therapeutic and diagnostic modalities together.

1 Introduction

Metal nanoparticles have promising application in photothermal therapy,[1] surface plasmon enhanced Raman scattering (SERS),[2] surface plasmon enhanced fluorescence,[3] because of their localized surface plasmon resonance (LSPR) properties. The electromagnetic waves interact with the surface conduction electrons of metal nanoparticle, producing a collectively coherent resonance, namely LSPR phenomenon.[4] Be confined to the metal nanoparticle, the localized surface plasmons can result in strong absorption, scattering and significant electric field enhancement around metal nanoparticle.[5,6]

Owing to tunable light absorption/scattering properties, metal nanostructures have been demonstrated as photothermal agent for cancer therapy recently. Photothermal therapy is the application of strong absorption phenomena, typically involving the conversion of light energy to localized heat that is used to deconstruct the cancer cells.[1] In therapy process, incident light can penetrate to depths of several centimeters through tissue in near-infrared region (650-950 nm),[7,8] where water and hemoglobin have weak absorption. Hence, 808 nm laser is widely used to research photothermal efficiency for in-vivo applications. When the LSPR peak of metal nanoparticle matches the incident light, photothermal conversion efficiency of nanoparticles can be improved efficiently. Based on this, Au nanoparticles with near-infrared (NIR) absorption were investigated for photothermal agent.[7] The central peak of LSPR can be tuned from the visible to near infrared regions by changing the size, shape and morphology of the Au nanoparticles.[9] Wyatt and co-workers suggest that the cytotoxicity of gold is negligible.[10] Coupling this with the fact that the gold is known to be resistant to oxidation and biologically inert,[11] it is justified that Au nanoparticles are an ideal material for photothermal therapy. Up to now, many groups make efforts to explore synthetic routes of different gold nanostructures, including nanosphere,[12] nanorod,[13] nanoprism,[14] nanocage[15] and nanostar.[16,17] The key of photothermal therapy is to improve the absorption intensity and photothermal transduction efficiency. Branched Au nanoparticle with the larger absorption cross section at the position of LSPR peak, is a novel photothermal nanostructure.[18,19] In addition, this kind of nanoparticles can produce strongly localized and enhanced electric field in the sharp and spiky region.

Recently, metal composite structures have attracted a great attention. The combination of therapeutic and diagnostic components into a nanostructure can monitor biological processes and achieve treatment at the same time. Such composite nanostructures allow for the imaging and detection

of targeted position, which improve the specificity and increase the efficacy of treatment.[2] Vo-Dinh et al.[2] synthesized Au nanostar and protoporphyrin IX composite structure combining Raman imaging and photothermal effect. Quan Li et al.[20] confined the photosensitizer (PS) methylene blue (MB) in the vicinity of Au nanorod, researching the role of the plasmonic effect in enhancing drug efficacy. Khlebtsov et al.[21] reported Au-Ag nanocage and Yb-2, 4-Dimethoxyhematoporphyrin nanocomposites. In previous studies, dyes are used as the fluorescence material in photothermal and fluorescent composites, which is not benefit for in vivo applications. Compared with traditional dyes, quantum dots (QDs) have unique properties. Narrow and size dependent emission spectrum, anti-photobleaching, and high brightness make QDs gain increasing interest in bio-labeling. Considering the low toxicity and the high fluorescent effect of QDs, CdTe/CdS/ZnS core-shell QDs were adopted.[22]

In this paper, Au NF@SiO_2@QDs structures were synthesized. Au nanoparticle core-shell composite structure combines therapeutic and diagnostic components in a nanostructure,[2] which have potential application in medical field. Silica is a widely used material for synthesizing concentric core-shell nanostructures.[23] Au NF coated by silica shell is efficient at enhancing stability and improving biocompatibility. In the process of experiment, the SPR peak of Au NFs was tuned to NIR region to match with the wavelength (808 nm) of laser by changing the amount of seed. Under resonance excitation, Au NF@SiO_2@QDs composites linking with antibody (AT) reveal high photothermal transduction efficiency. In addition, it was confirmed that Au NF@SiO_2@QDs-AT composites can targeted to the membrane of the MCF-7 and MDA-MB-231 breast cancer cells, serving as a fluorescent probe for labeling of cells. Therefore, Au NF@SiO_2@QDs nanoparticles will have great prospect in photothermal treatment and bio-labeling.

2 Experimental

2.1. Materials

Chloroauric acid ($HAuCl_4$, AR), sodium borohydride ($NaBH_4$, ⩾ 96.0%), cetyltrimethylammonium bromide (CTAB, ⩾ 99.0%), ascorbic acid (AA, ⩾99.7%), poly (vinyl pyrrolidone) (PVP, powder, Mw=10000), deionized water (18.25 MΩ·cm), N,N-dimethylformamide (DMF, 99.8%), tetraethyl orthosilicate (TEOS) (28.4% SiO_2, AR), ethanol (99.7%), ammonia (25-28% NH_3, AR), 3-aminopropyltrimethoxysilane (APS, Sigma) (98%), zinc chloride ($ZnCl_2$, 99%), cadmium chloride ($CdCl_2$.2.5 H_2O, 99%), thioacetamide (TAA, 99%), tellurium powder (99.999%), 2-propanol, 3-Mercaptopropionic acid (MPA), sodium hydroxide (NaOH, ⩾96.0%), rabbit anti-CK19 (Beijing biosynthesis biotechnology co., Ltd.), 1-Ethyl-3-(3-dimethylaminopropyl) carbodiimide hydrochloride (EDC), N-hydroxysuccinimide (NHS). 4',6-diamidino-2-phenylindole (DAPI). Cell culture media, supplements, MCF-7 and MDA-MB-231 breast cancer cells are all supplied by First Affiliated Hospital of Anhui Medical University. All chemicals were used without further purification.

2.2. Synthesis of Au nanosphere

Firstly, the synthetic methods about 3-nm Au nanospheres were similar to the one reported previously.[24] 0.6 mL of ice-cold $NaBH_4$ (10 mM) was added to the mixture of 10 mL of $HAuCl_4$ (0.25 mM) and CTAB (0.1 M). The solution was incubated for least 3 h at 30 °C. Secondly, 12 mL of water solution containing $HAuCl_4$ (0.25 mM) and CTAB (0.1 M), and 5 mL of AA (0.09 M) were mixed together. 0.3 mL as-prepared suspension liquid of Au nanospheres was added to the mixture solution to form larger nanospheres. After 1 min, this colorless solution turned into red. The product was spined down at 12 000 rpm for 45 min. At last, the product was dispersed in 1 mL pure water for further application.

2.3. Synthesis of PVP-stablized Au seed

200 μL as-prepared Au nanosphere solution was added to 6 mL of DMF solution containing $HAuCl_4$ (0.16 mM) and PVP (MW=10000) (0.21 M). Then the reaction solution was heated in oil bath at 80°C for 1 h with stirring. The product was used as seeds for the preparation of nanoflowers.

2.4. Synthesis of Au nanoflower

15 mL of DMF solution containing PVP (9 M) and 180 μL of $HAuCl_4$ was mixed.[25] Au seeds were then added under continuous stirring and allowed to react for 2 h. The product was rinsed for two times, and then dispersed in 20 mL of ethanol for further application.

2.5. Preparation of Au nanoflower@SiO_2

SiO_2 shell was grown on the surface of Au nanoflower by Stöber method. The detailed synthesis process was described as follow: 3 mL of water was added to as-prepared Au nanoflower ethanol solution. Then, 1mL of ammonia aqueous solution was introduced. Under vigorous stirring, 15 μL, 20 μL, 80 μL of mixture of APS and TEOS (the molar ratio was 2:1) was injected, respectively. The solution was washed with ethanol and dissolved in pure water for further application after 20 min.

2.6. Preparation of CdTe/CdS/ZnS QDs

NaHTe was prepared by 50 mg $NaBH_4$ and 80 mg Te added to 2 mL water. $CdCl_2$·2.5 H_2O and MPA was added to 100 mL pure water. Then the solution was adjusted to pH 8.5 by adding 0.5 M NaOH. After being deaerated with N_2 for 1h, NaHTe solution was added (Cd:Te:MPA=2:1:4.8). The mixture solution excluded oxygen for 5 h at 100 °C. The as-prepared CdTe QDs were washed with 2-propanol and dispersed in 5 mL of deionized water. 0.1 mmol $CdCl_2$·2.5 H_2O and 0.3 mmol MPA were added to 95 mL of water. Then solution was adjusted to pH 8.5 with 0.5 M NaOH. After adding 0.1 mmol TAA and CdTe QD solution, the mixture solution refluxed for

1h at 100 °C. The as-prepared CdTe/CdS QDs was washed with 2-propanol and dispersed in 5 mL of deionized water. 0.1 mmol $ZnCl_2$ and 0.3 mmol MPA were added to 95 mL. The mixture was adjusted to pH 8.5 with 0.5 M NaOH. Then 0.1 mmol TAA and CdTe/CdS QDs were added. The mixture was refluxed for 1h at 80 °C.[26,27]

2.7. Preparation of Au NF@SiO_2@QDs and covalent conjugation Au NF@SiO_2@QDs with antibody

100 μL QDs was added to Au NF@SiO_2 water solution. After 10-min ultrasound, the product was centrifuged and dissolved in PBS solution. 50 μL EDC (20 mg/mL) and 5 μL NHS (20 mg/mL) were added into PBS solutions of Au NF@SiO_2@QDs. All of the samples were incubated at 37 °C for 1 h in the table concentrator. 100 μL (0.1 mg/mL) of antibody was added to PBS solution. Then the mixture was incubated at 37 °C for 1 h. The product was finally washed with PBS solution for further application.

2.8. Photothermal effect of Au NF@SiO_2@QDs-AT

The MCF-7 breast cancer cells were seeded on 6-well culture plates in DMEM medium and maintain overnight at 37°C in a humidified 5% CO_2 atmosphere. 100 μL Au NF@SiO_2@QDs-AT and the same amount of PBS solution were added into the medium, respectively. The cells were cultured for 3 h. Then cells were washed with PBS and irradiated by an 808-nm laser at a power density of 1.0 W/cm^2. Prior to viability staining, cells were cultured for 5 h at 37°C in a humidified 5% CO_2 atmosphere. The viability state of cells was researched by dark-field microscope.

2.9. Fluorescence labeling effect of Au NF@SiO_2@QDs

The MCF-7 breast cancer cells and MDA-MB-231 breast cancer cells were cultured on coverslips in DMEM medium containing 10% fetal bovine serum. The coverslips were carefully washed three times with PBS solution. Then, Au NF@SiO_2@QDs-AT composite structures were added onto these coverslips and incubated for 1h at 37°C. Prior to imaging, the coverslips were washed three times with PBS. Cell images were observed by a fluorescence microscope.

2. 10. Characterization

The morphological information of nanoparticles was conducted by transmission electronic microscopy (TEM, JEOL, JEM-2010) and scanning electron microscope (SEM, JSM-6700F). The UV-visible absorbance spectra were measured by using an UV-3600 UV-VIS-NI spectrophotometer. Photoluminescence spectra were obtained by using an F-4600 fluorescence spectrophotometer. Cells were imaged using Olympus IX 73 fluorescence microscope and Leica SP5 laser scanning confocal microscope.

3. Results and discussion

The procedure for the production of composite structures is shown schematically in Fig. 1. The reduction method of $NaBH_4$ was used to produce small Au seed. Then the larger Au nanospheres were synthesized with the reduction of AA. As is well known, the growth processes of nanoparticle comply with the rules of kinetics and thermodynamics: The small Au nanospheres and larger Au nanospheres were all synthesized at ambient temperature. The thermal stability is not strong. After stored for a few days, the nanoparticles will grow further. It is not benefit for us to tune the SPR peak of nanoflowers by controlling the amount of seeds. Therefore we introduced a synthesis process of PVP-stabilized Au nanoparticles using weak reducing agent in the environment of heating. The product has good stability at room temperature, which was appropriate as seeds of Au NFs. After producing a batch of seeds, a few of nanoflower samples can be synthesized to form a small database by adding different amount of seeds. The SPR peak of nanoflowers can be easily tuned to the target wavelength position according to this database. Carboxyl groups terminated QDs were assembled to the surface of Au NF@SiO_2. Finally, antibodies were further coupled to the surface of Au NF@SiO_2@QD_S in the presence of EDC and

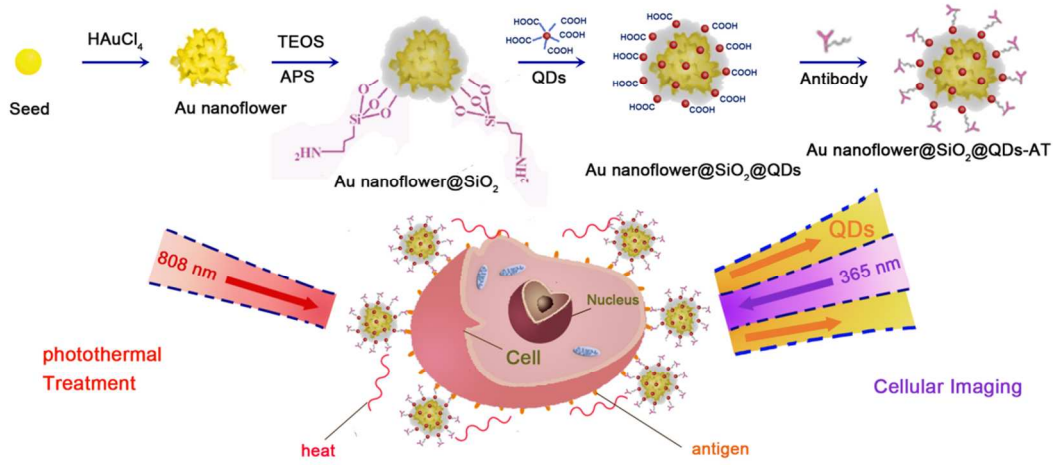

Fig. 1 Schematic illustrating the synthesis of Au nanoflowers@SiO_2@QDs composite structures.

NHS as activating reagents. Au NF@SiO_2@QDs composites had photothermal and fluorescent effect, which have potential application in photothermal treatment and celluar imaging.

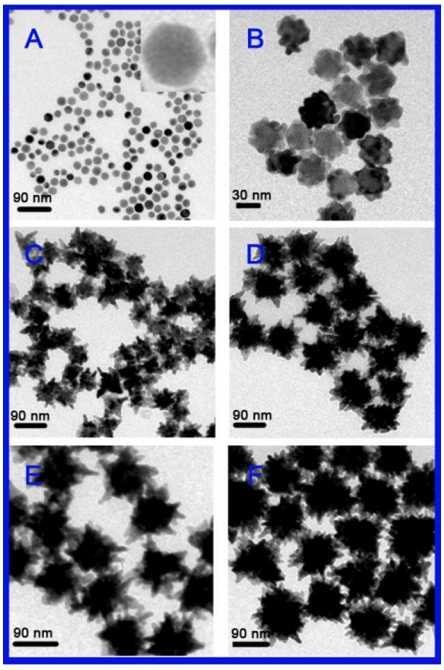

Fig. 2 TEM images of (A) Au seeds, and Au nanoflowers made from different volume of seeds： (B) 2000 μL, (C) 1300 μL, (D) 650 μL, (E) 520 μL and (F) 260 μL, respectively.

Gold nanoflowers were prepared by the method of seed growth. PVP-stablized Au nanoparticles were adopted as seed, which were shown in Fig. 2A. Au nanoflowers samples with five different sizes were prepared by adding different amount of seeds. Fig. 2B-F show the TEM images of nanoflowers with different sizes, respectively. These nanoflowers have relatively uniform size and shape distribution. The average sizes of five samples were measured to be 40 nm, 80 nm, 120 nm, 130 nm，150 nm, respectively. The volume of seeds are gradually reduced from 2000 μL, 1300 μL, 650 μL, 520 μL to 260 μL.

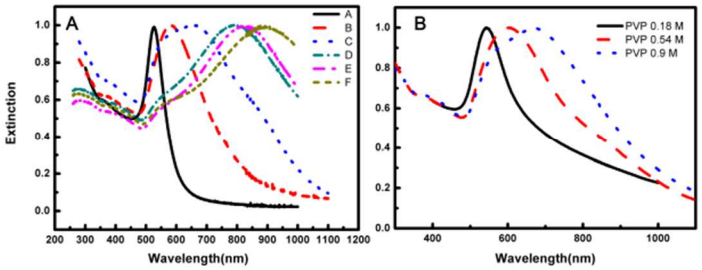

Fig. 3 (A) Normalized absorption spectra of Au seeds and Au nanoflowers. From left to right is the absorption of samples corresponding to A-F in Fig. 2. (B) Extinction spectra of Au nanoflowers samples grown in the solution with different concentration of PVP.

Fig. 3A shows the absorption spectra of five samples and seeds. The absorption peak of nanoflowers can be tuned from visible light region to near-infrared region. The plasmon resonance wavelength of seed is 527 nm. As the reduction of seed amount, the plasmon resonance wavelengths of five Au nanoflowers samples are varied from 581 nm, 659 nm, 792 nm, 829 nm to 890nm. The SPR peak is closely related to local electric field distribution of metal nanoparticle. The amplitude of local field influences the energy of SPR that corresponds to the SPR wavelength. The charges located at the sharp corners of each nanoparticle. The distance between positive and negative charges equivalent charge center increases with increasing the nanoparticle size, which cause the increase of the plasmons restoring force and the shift of SPR peak. [28] In order to research the influence of PVP concentration on the absorption peak of product, three samples were synthesized by changing the concentration of PVP only. Fig. 3 B shows the absorption spectra of the three samples. The absorption peaks of product generate blue shift with reducing PVP concentration. With further decrease of PVP concentration, the absorption peak can approach the peak of seed. The mechanism should be that high ratios of vinylpyrrolidone monomeric units to Au atoms lead to a rapid, kinetically controlled and preferential growth along certain crystalline facets.[29] Nanoparticle will grow along the crystalline facets with the lower surface free energies based on thermodynamic control. With the decrease of PVP concentration, the preferential growth processes of nanoparticles were restrained, which inhibit the form of branched nanostructure and benefit the form of nanostructure that is similar to spherical shape nanoparticle.

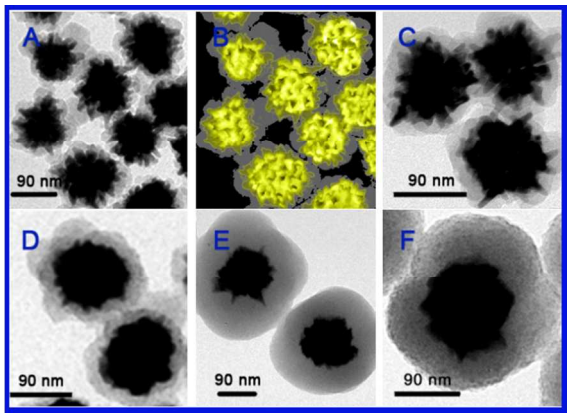

Fig. 4 (A) TEM image and (B) schematic plot of Au nanoflowers@SiO_2, respectively. (C, E) TEM images of the obtained Au nanoflowers@SiO_2 with different shell thickness. (D, F) TEM images of Au nanoflowers@SiO_2@QDs corresponding different thickness of silica shell.

To further demonstrate the core-shell structure of Au NF@SiO_2 and Au NF@SiO_2@QDs, the morphologies of these nanoparticles were conducted by TEM images. Fig.4 (A, B) show the TEM image and schematic plot of Au NF@SiO_2 (the

silica shell thickness is about 9 nm) composite structure. Fig. 4 (C, E) show the silica shell thickness of Au NF@SiO_2 to be about 16, 65 nm, respectively. Corresponding Au NF@SiO_2@QDs composite nanoparticles were showed in Fig. 4 (D, F). It can be observed that these nanoparticles are homogeneous core-shell structures. The thickness of the silica shell increased with the increasing of TEOS amount. Surface-protective agents play a significant in preventing aggregation and surface-modifying function for further application. Herein, aminopropyltrimethoxysilane (APTMS) was chosen to modify the surface of SiO_2, which can provide amino group for combining negatively charged QDs.

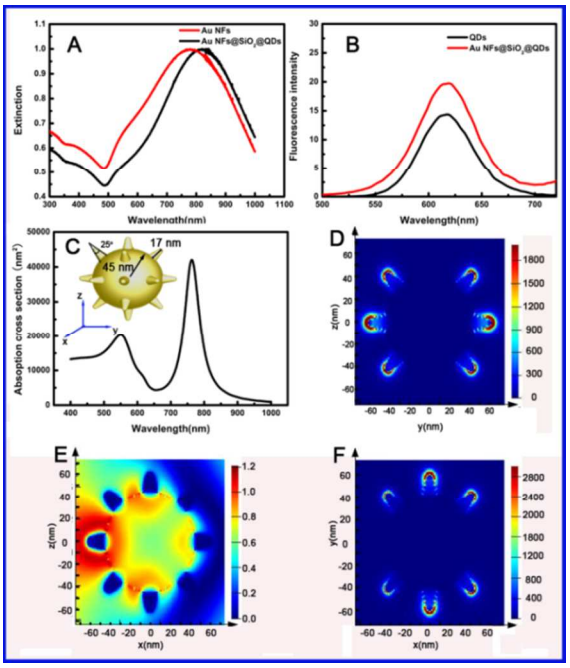

Fig.5 (A) Extinction spectra of Au NFs (red line) and Au NF@SiO_2@QDs (black line). (B) Fluorescence spectra of QDs (black line) and Au NF@SiO_2@QDs (red line). (C) Absorption cross section of Au NF model, (inset) simplified model. Simulated electric field intensity distribution (D) in yz plane at x=0, (E) in xz plane at y=0, (F) in xy plane at z=0. The incidence direction is along x axis. The polarization of the incident light is along y axis.

Silica shell was used to control the distance between the Au nanoflower and QDs, which prevents fluorescence quenching phenomena of QDs caused by charge transfer. In general, PL quenching appears when the distance between metal nanoparticle and fluorophores is less than 5 nm. PL enhancement is achieved at larger distance (7-20 nm).[30,31] So, Au NF@SiO_2@QDs nanoparticles with silica shell of 16 nm were used in the subsequent experiment. The SPR peak of Au NF@SiO_2@QDs has 36 nm redshift compared with that of Au NF due to the change of dielectric environment (Fig. 5 A). The SPR peak of Au NF was tuned from 779 nm to 815 nm, which matches with the 808 nm laser. The amount of red-shifting is related with the thickness of silica shell. In order to match the absorption peak of Au NF@SiO_2@QDs with the wavelength of laser, the SPR peak of Au NFs and the amount of TEOS added should be considered at the same time. Fig. 5 B shows the fluorescence spectra of QDs before and after connecting to Au NF@SiO_2 by self-assembly, with the excitation of 365 nm light. It was clear that Au NF@SiO_2@QDs has efficient PL enhancement (up to an enhancement factor of 1.4), compared with pure QDs. Generally, PL enhancement contributes to two mechanisms. One is excitation enhancement caused by efficient enhancement of the local field associated with the resonance coupling between LSP of metal and incident electromagnetic field，which can induce the efficient increase of absorption and excitation rate. The other is the increase of the radiative decay rate caused by the resonance coupling between LSP of metal nanoparticles and fluorophores emission.[31] The LSPR bands of Au NFs have large degree of spectral overlap with the emission wavelength of QDs (615 nm). Therefore, PL enhancement should be caused by the second mechanism.

With the aim of explaining the excellent photothermal effect of Au NF, the electric field distribution is calculated using three-dimensional finite-difference time-domain method (FDTD). The boundary conditions of the computational domain were set to perfectly matched layer absorbing boundaries. The simulation region is 1μm×1μm×1μm, and the cell size is 1 nm×1 nm×1 nm. A linearly polarized plane wave with 780 nm wavelength irradiates Au NF along x axis. Au NF was simulated by employing a geometrical model consisting of a central sphere with eighteen tapered cylinder that possesses a round tip (see inset in Fig. 5 C). Tip radius and cone angle were set to 3.5 nm and 25°, respectively. All the parameters chosen here are consistent with the average value obtained in experiment (see Fig.4 C). As seen in Fig. 5 C, the absorption cross section spectrum of the simplified model matches with the experimental result. There are two characteristic LSPR peaks. A very intense peak is around 780 nm, and a weaker peak is around 550 nm. The corresponding E-field distribution calculated with FDTD method was shown in Fig. 5 D-F. The largest local electric field is accumulated on the tips of Au NF, thereby providing large field enhancement. In addition, there is a large absorption cross section , making Au NF an ideal material for photothermal therapy.

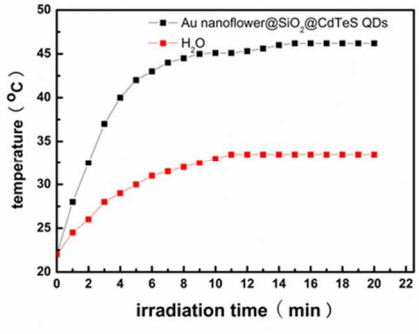

. Fig.6 Temperature plot as a function of irradiation time.

The temperature-time curve was measured in order to research the photothermal conversion efficiencies of Au NF@SiO_2@QDs composites. As shown in Fig. 6, the temperature of Au composites solution (0.102 mmol/L) increased rapidly in the first five minutes and gradually reached a plateau of 46.2 ^oC with irradiation of an 808-nm laser at a power density of 1.0 W/cm^2. As a control group, the temperature of PBS solution increased with a slower rate under similar conditions. Ultimately, the temperature of control group remains stable around 33.5 ^oC.

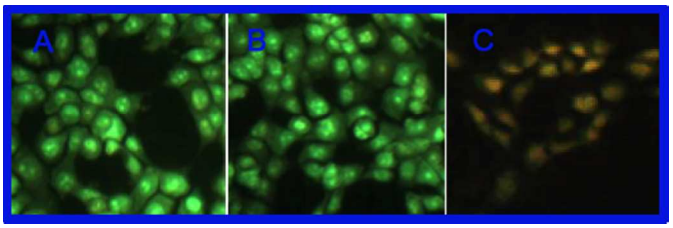

Fig.7 Viability staining of the MCF-7 breast cancer cells incubated with (A) PBS solution and with irradiation of laser, (B) Au NF@SiO_2@QDs-AT and without irradiation, and (C) Au NF@SiO_2@QDs-AT and with irradiation of laser.

Viability staining of the MCF-7 breast cancer cells was used to verify photothermal effect of Au NF@SiO_2@QDs. The experiment group was incubated with Au NF@SiO_2@QDs-AT (Fig. 7 C). The control group one was incubated with the same volume of PBS solution (Fig. 7 A). The control group two was incubated with Au NF@SiO_2@QDs-AT (Fig. 7 B). The experiment group and the control group one were irradiated by an 808-nm laser at a power density of 1.0 W/cm^2. The control group two keeps at the same environment with the experiment group but without the irradiation of laser. After culturing for 5 h, cells were studied by viability staining. Fluorescent terminating agent (containing metanil yellow and ethidium bromide) was added to the tree groups. Metanil yellow can react with cell membrane and dyed the membrane of live cells green. Ethidium bromide can penetrate through the cell membrane that was damaged to make cell nucleus turn orange-red. Therefore, orange-red stained cells are dead cells, and green-stained cells are live cells. As shown in Figure 7, the photothermal effect of Au NF@SiO_2@QDs is obvious. The experiment group appears cell detachment due to heating effect. The temperature of this group is up to the cytotoxic level that is 43-48^oC. Protein denaturation takes place.[32] The control group one and two had hardly any cell death phenomena. The only difference between control group one and experiment group is the absence of Au NF@SiO_2@QDs-AT. The two groups have the same condition of irradiation. The viability result of the two groups suggests that the laser intensity is hardly harmless to cells without Au NRs in the experiment. The viability of cell in control group two didn't drop, which testify that the introduction of Au NF@SiO_2@QDs-AT is not the direct reason of the death of cell in experiment group. Therefore, these results show that the photothermal effect of Au NF@SiO_2@QDs terminates cells.

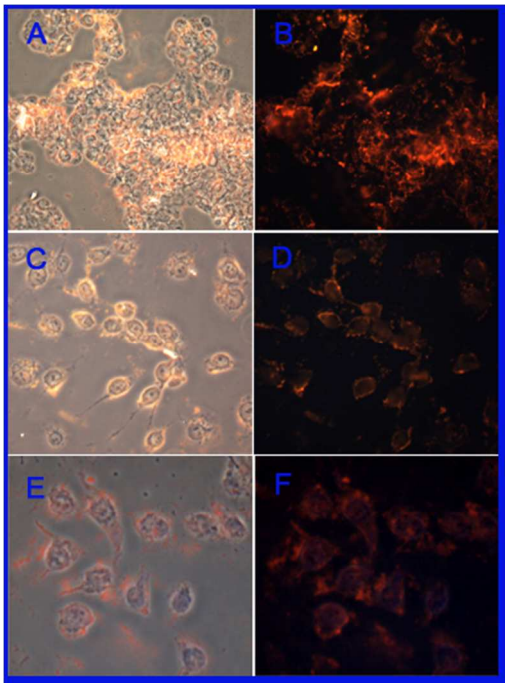

Fig. 8 Bright-field image of (A) the MCF-7 breast cancer cells with treatment of Au NF@SiO_2@QDs-AT, (C) and (E) the MDA-MB-231 breast cancer cells with treatment of Au NF@SiO_2@QDs-AT and Au NF@SiO_2@QDs-AT/DAPI, respectively. (B), (D) and (F) fluorescence image corresponding to (A), (C) and (E), respectively.

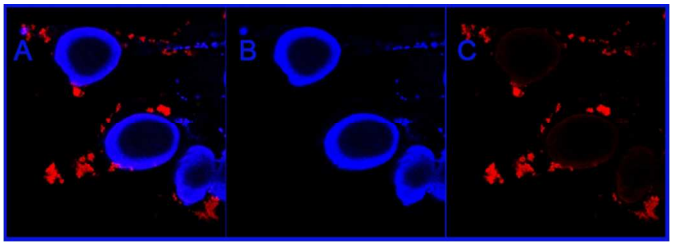

Fig. 9 Image of the MDA-MB-231 breast cancer cells taken on the condition of (A) red and blue, (B) blue, (C) red channel output.

Next, Au NF@SiO_2@QDs nanoparticles were applied for cellular imaging. The images of the cell were collected after being stained with composite structure. Fig. 8 (A, B) show the bright-field image and the fluorescence image of the MCF-7 breast cancer cells. The bright-field image and the fluorescence image of the MDA-MB-231 breast cancer cells were shown in Fig. 8 (C, D). Fluorescence images of the MDA-MB-231 breast cancer cells clearly indicate that ultraviolet irradiated cells emit strong red fluorescence. Subsequently, they were stained with DAPI to visualize the nuclei. The bright-field image and the fluorescence image of the MDA-MB-231 breast cancer cells with the treatment of Au NF@SiO_2@QDs-AT and DAPI were shown in Fig. 8 (E, F). In order to observe the structure of the MDA-MB-231 breast cancer cells more clearly, laser scanning confocal microscope was used. The fluorescence

confocal images were shown in Fig. 9 (A, B, C), which showed three situations of two channel output. The red channel corresponds to QDs, the blue channel is DAPI. The images were obtained under 365 nm UV excitation. As is shown in Fig. 9 B, the nuclei were stained in blue. Fig. 9 C shows definitely that the MDA-MB-231 breast cancer cells emit red fluorescence, indicating that Au NF@SiO_2@QDs successfully targeted the membrane of the cells.

Conclusions

PVP stabilized Au NFs with tunable SPR peak were synthesized. Silica was deposited onto the surface of Au NFs through optimized Stöber method, acting as the medium of Au NFs and quantum dots. Numerical simulation shows that Au NFs with enhanced local electric field and large absorption cross section are suitable for photothermal therapy. The photothermal and fluorescent properties of Au NF@SiO_2@QDs nanoprobe were demonstrated on the MCF-7 and MDA-MB-231 breast cancer cells. Photothermal test shows that the nanoprobes can successfully convert NIR irradiation to thermal energy that causes the death of cancer cells. Fluorescence images intuitively indicate that nanoprobes can target the membrane of breast cancer cells and emit strong fluorescence. Combined together, it can be concluded that Au NF@SiO_2@QDs multi-functional nanoprobes have significant application prospect in photothermal treatment and cellular imaging.

Acknowledgements

This work was supported by the National Natural Science Foundation of China (No. 51272246 and No.81172082), and the Fundamental Research Funds for the Central Universities of China (Grant No. 2030000001)

Notes and references

a Department of Physics, University of Science and Technology of China， Hefei, Anhui 230026，Tel: +86 551 63607574; E-mail: xlxu@ustc.edu.cn.
b Center Laboratory, First Affiliated Hospital of Anhui Medical University, Hefei, Anhui, E-mail: lx-zhu@163.com.

1 J. Li, J. Han, T. Xu, C. Guo, X. Bu, H. Zhang, L. Wang, H. Sun, B. Yang, *Langmuir*, 2013, **29**, 7102-7110.
2 A.M. Fales, H. Yuan, T. Vo-Dinh, *Mol. Pharmaceutics*, 2013, **10**, 2291-2298.
3 T. Zhao, K. Yu, L. Li, T. Zhang, Z. Guan, N. Gao, P. Yuan, S. Li, S. Q. Yao, Q.-H. Xu and G. Q. Xu**,** *ACS appl. Mater. Inter.***,** 2014**, 6,** 2700-2708**.**
4 W. Deng, E. M. Goldys, *Langmuir*, 2012, **28**, 10152-10163
5 A. V Zayats, I. I Smolyaninov, *J. Opt. A*, 2003, **5**, S16-S50
6 J Zuloaga, P Nordlander , *Nano lett.*, 2011, **11**, 1280-1283.
7 Y. Wang, K. C. L. Black, H. Luehmann, W. Li, Y. Zhang, X. Cai, D. Wan, S.-Y. Liu, M. Li, P. Kim, Z.-Y. Li, L. V. Wang, Y. Liu, Y. Xia, *ACS Nano*, 2013, **7**, 2068-2077.
8 M. D. Blankschien, L. A. Pretzer, R. Huschka, N. J. Halas, R. Gonzalez, M. S. Wong, *ACS Nano*, 2013, **7**, 654-663.
9 A.J. Mieszawska, W.J. Mulder, Z.A. Fayad, D.P. Cormode, *Mol. pharmaceutics*, 2013, **10**, 831-847.
10 C. Wang, Z. Ma, T. Wang, Z. Su, Adv. *Funct. Mater.*, 2006, **16**, 1673-1678.
11 V.W.K. Ng, R. Berti, F. Lesage, A. Kakkar, *J. Mater. Chem. B*, 2013, **1**, 9-25.
12 C. Li, D. Li, G. Wan, J. Xu, W. Hou, *Nanoscale Res. Lett.* 2011, **6**, 440
13 A. Umar, S.-M. Choi, *J. Phys. Chem. C*, 2013, **117**, 11738-11743.
14 C. Bao, N. Beziere, P. del Pino, B. Pelaz, G. Estrada, F. Tian, V. Ntziachristos, J.M. de la Fuente, D. Cui, *Small*, 2013, **9**, 68-74.
15 J. Chen, J.M. McLellan, A. Siekkinen, Y Xiong, Z.-Y. Li, Y. Xia, *J. Am. Chem. Soc.*, 2006, **128**, 14776-14777
16 I. Baginskiy, T.-C. Lai, L.-C. Cheng, Y.-C. Chan, K.-Y. Yang, R.-S. Liu, M. Hsiao, C.-H. Chen, S.-F. Hu, L.-J. Her, D.P. Tsai, *J. Phys. Chem. C* , 2013, **117**, 2396-2410.
17 S. Wang, P. Huang, L. Nie, R. Xing, D. Liu, Z. Wang, J. Lin, S. Chen, G. Niu, G. Lu, X. Chen, *Adv. Mater.*, 2013, **25**, 3055-3061.
18 R. Rodríguez-Oliveros, J.A.Sánchez-Gil, *Opt Express*, 2012, **20**, 621-626.
19 R. Rodríguez-Oliveros, J. A. Sánchez-Gil, Opt. Express, 2012, 20, 621-626.
20 Z. Chu, C. Yin, S. Zhang, G. Lin, Q. Li, *Nanoscale*, 2013, **5**, 3406-3411.
21 B. Khlebtsov, E. Panfilova, V. Khanadeev, O. Bibikova, G. Terentyuk, A. Ivanov, V. Rumyantseva, I. Shilov, A. Ryabova, V. Loshchenov, N. G. Khlebtsov, *ACS Nano*, 2011, **5**, 7077-7089.
22 H. Huang, J. Liu, B. Han, C. Mi, S. Xu, *J. Lumin.*, 2012, **132** 1003–1009.
23 T. Chen, G. Chen, S. Xing, T. Wu, H. Chen, *Chem. Mater.*, 2010, **22**, 3826-3828.
24 X. Ye, C. Zheng, J. Chen, Y Gao, C. B. Murray, *Nano Lett.*, 2013, **13**, 765-771.
25 C.G. Khoury, T. Vo-Dinh, *J. Phys. Chem. C*, 2008, **112**, 18849-18859.
26 L. Li, H. Qian, N. Fang, J. Ren, *J. Lumin.*, 2006, **116**, 59-66
27 Z. Li, C. Dong, L. Tang, X. Zhu, H. Chen, J. Ren, *Luminescence*, 2011, **26**, 439-448.
28 L. Yuan, J. Zhu, Y. Ren and S. Bai, *J. Nanopart. Res.*, 2011, **13**, 6305-6312
29 I. Pastoriza-Santos and L. M. Liz-Marzán, *Adv. Funct. Mater.*, 2009, 19, 679-688.
30 N. Liu, B. S. Prall, and V. I. Klimov, J. AM. CHEM. SOC., 2006,128, 15362-15363.
31 K. Sugawa, T. Tamura, H. Tahara, D. Yamaguchi, T. Akiyama, J. Otsuki, Y. Kusaka, N. Fukuda, H.Ushijima, *ACS Nano*, 2013, **7**, 9997-10010.
32 L. M. Maestro, P. Haro-Gonzalez, A. Sanchez-Iglesias, L. M. Liz-Marzan, J. Garcia Sole and D. Jaque, *Langmuir*, 2014, 30, 1650-1658.